



Midbrain dopamine neurons arbitrate OCD-like behavior

Jinwen Xue^a, Dandan Qian^a, Bingqian Zhang^b, Jingxuan Yang^a, Wei Li^a, Yifei Bao^a, Shi Qiu^a, Yi Fu^a, Shaoli Wang^{a,c}, Ti-Fei Yuan^{b,1}, and Wei Lu^{a,c,d,1}

Edited by Xiaoke Chen, Stanford University, Stanford, CA; received May 2, 2022; accepted September 28, 2022 by Editorial Board Member Hee-Sup Shin

The neurobiological understanding of obsessive-compulsive disorder (OCD) includes dysregulated frontostriatal circuitry and altered monoamine transmission. Repetitive stereotyped behavior (e.g., grooming), a featured symptom in OCD, has been proposed to be associated with perturbed dopamine (DA) signaling. However, the precise brain circuits participating in DA's control over this behavioral phenotype remain elusive. Here, we identified that DA neurons in substantia nigra pars compacta (SNc) orchestrate ventromedial striatum (VMS) microcircuits as well as lateral orbitofrontal cortex (IOFC) during self-grooming behavior. SNc-VMS and SNc-IOFC dopaminergic projections modulate grooming behaviors and striatal microcircuit function differentially. Specifically, the activity of the SNc-VMS pathway promotes grooming via D1 receptors, whereas the activity of the SNc-IOFC pathway suppresses grooming via D2 receptors. SNc DA neuron activity thus controls the OCD-like behaviors via both striatal and cortical projections as dual gating. These results support both pharmacological and brain-stimulation treatments for OCD.

neural circuits | dopaminergic modulation | SNc | excessive self-grooming | OCD

Obsessive-compulsive disorder (OCD) is characterized by unwanted distressing thoughts (obsessions) and repetitive acts (compulsions), with severe disruption of daily activities (1, 2). Recent evidence suggests that various structures, such as the cortex (3–5), striatum (6–9), hypothalamus (10), hippocampus (11, 12), amygdala (13–15), and even spinal cord (16), contribute to the pathology of OCD. Imbalanced cortical-striatal activities, such as the dynamics in cortico-striato-thalamo-cortical (CSTC) circuit are recognized as the core neurobiological substrate for OCD (17–19). Specifically, hyperactivity in the medial subregion of the orbitofrontal cortex (containing medial and ventral orbital; labeled vmOFC henceforth) and ventromedial striatum (VMS) is implicated in the expression of repetitive behaviors (20–24). Rodent self-grooming can be considered as a correlate of human complex repetitive, self-directed, and sequentially patterned behaviors. Repetitive cortico-striatal stimulation that strengthens vmOFC-VMS functional connection can generate persistent OCD-like repetitive grooming behavior (25). By contrast, activating the lateral orbitofrontal cortex (IOFC)-striatal pathway prevents overexpression of both conditioned and spontaneous repetitive grooming (26). These previous studies implicate VMS's role in encoding the grooming state of the animal, potentially through balancing its microcircuitry neural activities.

Midbrain dopaminergic system is implicated in OCD-like behavior. Studies in rodents have shown that the activation of D1 receptor or D1-expressing neurons results in excessively stereotyped grooming (27, 28), whereas knocking out D1 receptor (D1R) reduces self-grooming bouts (29), suggesting that D1R signaling in the striatum may facilitate grooming. In clinical practice, dopamine antagonists have been used to augment the therapeutic effect of selective serotonin-reuptake inhibitors in patients with OCD (30). Unfortunately, the specific roles of dopamine receptors, as well as the precise brain circuits participating in dopaminergic regulations over the repetitive behavioral phenotype, remain unelucidated.

Here, we show that dopamine neurons in ventral substantia nigra pars compacta (SNc) bidirectionally modulate the grooming behavior through two independent long-range circuits and distinct dopaminergic receptor profiles, respectively. Our results indicate that pharmacological and optogenetic manipulations of the dopaminergic pathway activities are sufficient to restore normal behavior.

Results

Optogenetic Inhibition of SNc-VMS Projections Suppresses Excessive Self-Grooming in OCD Mice. We first generated mice with OCD-like repetitive self-grooming (termed OCD-like mice in the following context) via repetitively optogenetic stimulating OFC inputs to elevate activity in vmOFC-VMS projections with a protocol previously

Significance

Repetitive stereotyped behavior is a common symptom in various psychiatric disorders, such as obsessive-compulsive disorder (OCD). The midbrain dopaminergic system has been implicated in this phenotype, but the precise location and circuit mechanism whereby it takes its action are unknown. Here, using an OCD animal model, we reveal that dopamine neurons in substantia nigra pars compacta (SNc) control the repetitive behavior via a dual gating mechanism from striatal and cortical projections. Our results suggest potential new targets in both pharmacological and brain-stimulation treatments for OCD.

Author affiliations: ^aMinister of Education (MOE) Key Laboratory of Developmental Genes and Human Disease, School of Life Science and Technology, Southeast University, Nanjing 210096, China; ^bShanghai Key Laboratory of Psychotic Disorders, Shanghai Mental Health Center, Shanghai Jiao Tong University School of Medicine, Shanghai 200030, China; ^cDepartment of Neurosurgery, Huashan Hospital, Institute for Translational Brain Research, State Key Laboratory of Medical Neurobiology, MOE Frontiers Center for Brain Science, Shanghai Medical College of Fudan University, Shanghai 200032, China; and ^dCo-innovation Center of Neuroregeneration, Nantong University, Nantong 226001, China

Author contributions: W. Lu and T.-F.Y. designed research; J.X., D.Q., B.Z., J.Y., W. Li, Y.B., S.Q., and Y.F. performed research; J.X., S.W., T.-F.Y., and W. Lu analyzed data and wrote the paper.

The authors declare no competing interest.

This article is a PNAS Direct Submission. X.C. is a guest editor invited by the Editorial Board.

Copyright © 2022 the Author(s). Published by PNAS. This open access article is distributed under Creative Commons Attribution-NonCommercial-NoDerivatives License 4.0 (CC BY-NC-ND).

¹To whom correspondence may be addressed. Email: luwei@seu.edu.cn or tifei.yuan@smhc.org.cn.

This article contains supporting information online at <http://www.pnas.org/lookup/suppl/doi:10.1073/pnas.2207545119/-DCSupplemental>.

Published November 7, 2022.

reported (25) (Fig. 1 *A* and *B*). In brief, we stereotactically injected an adenovirus-associated vector (AAV) carrying the gene encoding channelrhodopsin (ChR2) fused to an enhanced red fluorescent protein (mCherry) into the left vmOFC to specifically express ChR2 in glutamatergic neurons and implanted optic fiber just above left VMS for axon terminal stimulation (Fig. 1 *B*, *Left* and *SI Appendix*, Fig. S1). Then, repetitive 473-nm stimulations (10 ms, ~5 mW) at 10 Hz for 5 min were delivered to left vmOFC–VMS projections for 5 consecutive days in these awake-behaving mice. Digital video was employed to record grooming behavior (Fig. 1*A*), which was subsequently scored by blind raters for 5 min before (pre), during (stim), and after (post) stimulation. Consistent with the previous study (25), we detected a significant increase in grooming time 2 wk after repeated stimulation (Fig. 1 *B*, *Right*). Thus, the repeated stimulations established a mice model with OCD-like excessive self-grooming, as previously reported (25).

We then manipulated midbrain dopamine neurons (DANs) from either SNc or ventral tegmental area (VTA), the major midbrain DAN-containing regions, to investigate their potential roles in the regulation of excessive self-grooming in OCD-like mice. We expressed the opsin (eNpHR) selectively in DANs in SNc or VTA, using two viral vectors to accomplish this (*SI Appendix*, Fig. S1*E*): the first one expressed Cre recombinase under the control of tyrosine hydroxylase (TH) promoter fragment, while the second one expressed a Cre-recombinase-dependent opsin needed (31) (Fig. 1 *C* and *E*). We injected the two viral vectors in a 1:2 mixture into VTA or SNc. With this technique, we expressed eNpHR3.0 selectively in DANs at VTA or SNc in OCD-like mice (Fig. 1 *C* and *E*). We then delivered 593-nm optogenetic stimulations (~5 mW, 5 min) at VMS through optic fiber implanted to inhibit the activity of axon terminals from either of the two brain regions on day 22 (D22) (separated experiments in Figs. 2*L*, 3 *B–E*, and 6*I* were also performed at D22). We found that photoinhibition of the activity of projection terminals from SNc rapidly and reversibly suppressed the enhanced grooming time in OCD-like mice (Fig. 1*D* and *SI Appendix*, Fig. S2). By contrast, photoinhibition of VTA–VMS projection terminals failed to induce any effect on grooming time (Fig. 1*F* and *SI Appendix*, Fig. S2). These results indicate that dopaminergic inputs from SNc, but not VTA, facilitates OCD-like repetitive behavior. Moreover, electrophysiological results *in vivo* show that the firing frequency of DANs in SNc increased from 8.254 to 20.44 Hz after consecutive 5-d photoactivation of VMO–VMS (*SI Appendix*, Fig. S3 *A* and *B*).

To examine the specificity of SNc–dopamine control, we further examined the effect of photoinhibition of SNc–VMS on mobility and anxiety, two behaviors that can affect the expression of self-grooming. Our results reveal that photoinhibition of SNc–VMS failed to exhibit any effect on mobility and anxiety (*SI Appendix*, Fig. S4 *A–D*), indicating that SNc’s dopamine control is specific for OCD-like behavior. In addition, photoinhibition of SNc–VMS failed to exhibit any effect on spontaneous grooming in normal mice (*SI Appendix*, Fig. S5 *A–C*).

SNc-IOFC Circuit Gates OCD-like Behavior. SNc DANs project to multiple brain regions. To explore possible alternative pathways originating from SNc, we employed anterograde tracing with mixed AAV containing TH-Cre and EF1α-DIO-C1V1-EYFP to selectively expressed C1V1 and EYFP in DANs in SNc (Fig. 2*A*). Two weeks postinjection, EYFP staining was seen in both SNc DAN cell bodies and anterogradely labeled axons projecting to IOFC, suggesting the connection between SNc and IOFC (Fig. 2*B*).

To our knowledge, this SNc to IOFC projection has not been previously reported (32). We therefore further verify the observation using three complementary retrograde tracing methods. We, respectively, microinfused the retrograde tracer cholera toxin subunit B (CTB-555; Fig. 2 *C* and *D*, and *SI Appendix*, Fig. S6*A*), retrobeads (Fig. 2 *E* and *F* and *SI Appendix*, Fig. S6*B*), or retro AAV TH-Cre virus (Fig. 2 *G* and *H*) unilaterally in the IOFC of separate cohorts of mice and performed immunofluorescence staining of SNc to examine whether retrogradely labeled neurons in SNc are also TH-positive neurons. Consistent with our anterograde tracing results, all the labeled neurons with three retrograde tracing methods were found largely in the same region of SNc and specifically in the ipsilateral ventral region of the SNc.

To investigate whether the SNc DANs targeting VMS and IOFC belong to one or two different cell populations, we perform retrograde tracing from both regions with two different retro AAVs (Fig. 2*I*). We took advantage of different but specific recognition capability of the Cre-Loxp and Flp-FRT systems by injecting EF1α-DIO-mCherry and EF1α-fDIO-EYFP (1:1 mixture) into SNc and retro AAV TH-Cre and retro AAV TH-FLP into IOFC and VMS, respectively. The two different retro AAVs traveled retrogradely toward the somata of DANs under the TH promoter and led to either GFP or mCherry expression in SNc DANs. We successfully traced 1,940 DANs in SNc in total (obtained from five mice). Our results revealed a detailed percentage of DANs in SNc only projecting to VMS, to IOFC, and to both regions (Fig. 2 *J* and *K*), suggesting SNc DANs targeting the VMS and IOFC may largely represent two different populations.

This verified SNc–IOFC projection drew our attention, as IOFC has been reported to regulate OCD-like compulsive behaviors via its projections to VMS (26, 33). These studies demonstrate that optogenetic stimulation of IOFC and its terminals in the striatum restores behavioral response inhibition (26). Hence, the direct SNc–IOFC projection we observed here raises the possibility that, in addition to SNc–VMS’s crucial role in self-grooming regulation, SNc may take an additional role in self-grooming regulation via SNc–IOFC–VMS “detour”. To examine this possibility, in a separate set of experiments, we injected mixed AAV into SNc to express C1V1 in SNc DANs and implanted optic fiber in IOFC of OCD-like mice (*SI Appendix*, Fig. S1*B*). We found that 532-nm optogenetic stimulation (eight pulses at 30 Hz, 5-ms pulse width, every 5 s) on SNc axon terminals in IOFC reversed the enhancement in grooming time (Fig. 2*L* and *SI Appendix*, Fig. S2), suggesting that SNc DANs ameliorate OCD-like behavior through SNc–IOFC cortical projections. Moreover, photoactivation of SNc–IOFC failed to exhibit any effect on mobility and anxiety (*SI Appendix*, Fig. S4 *E–H*) or spontaneous grooming in normal mice (*SI Appendix*, Fig. S5 *D–F*).

To further confirm SNc pathways’ gating roles, we performed the opposite manipulation of the SNc pathways. Optogenetic inhibition on the SN–IOFC pathway further increased the grooming time of OCD-like mice (*SI Appendix*, Fig. S7 *A* and *B*). On the other hand, although photoactivation of SNc–VMS projections did not exhibit any acute effect on grooming in OCD-like mice (*SI Appendix*, Fig. S7 *C* and *D*), 5-d chronic photoactivation of this pathway caused increased grooming (*SI Appendix*, Fig. S7*E*).

As the present OCD model was made by artificially repeated stimulation of cortico-striatal projection, it is debatable whether any of the conclusions based on the model can genuinely represent OCD etiology. To explore this, we next test the role of

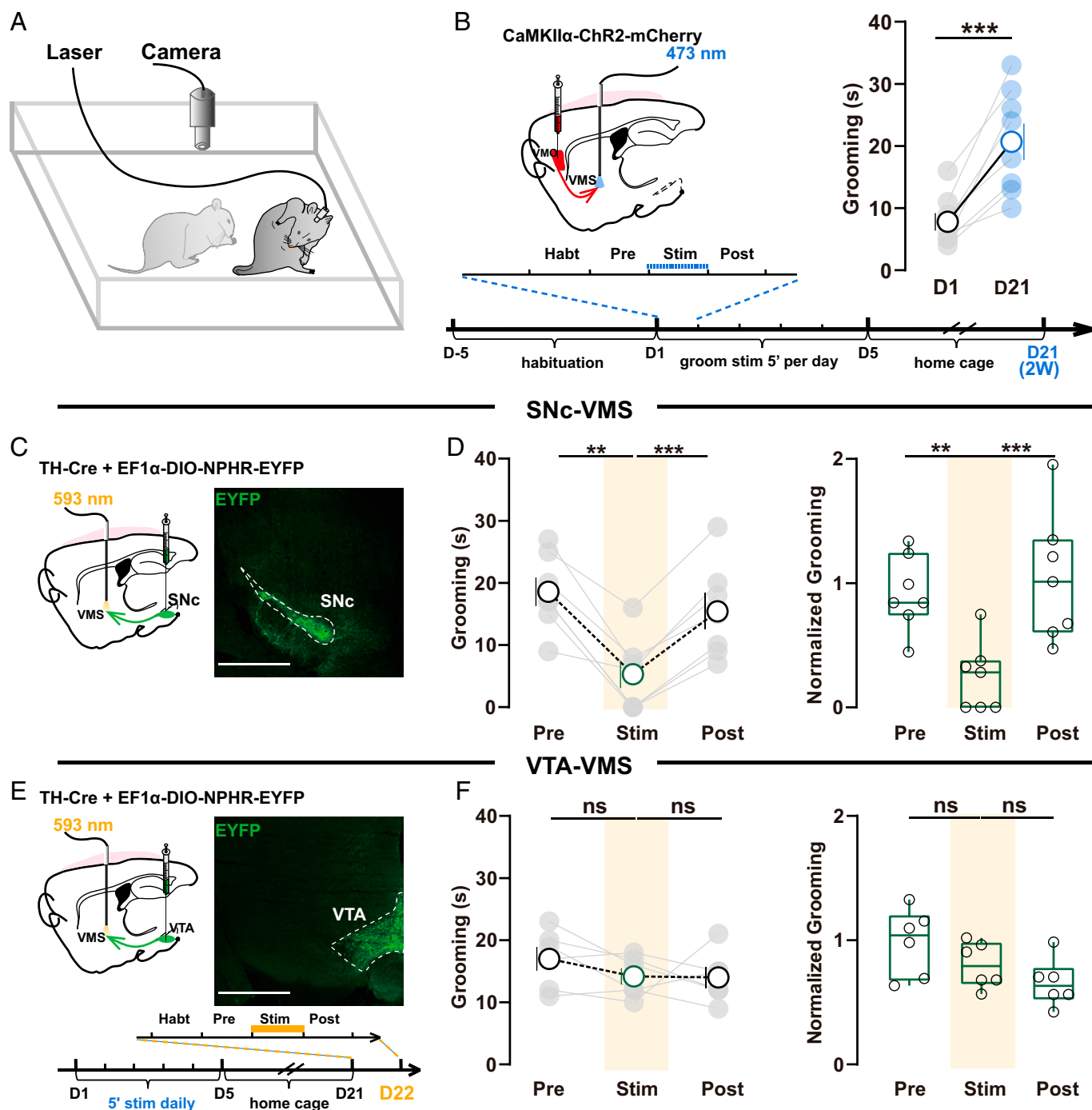


Fig. 1. Inhibition of SNC-VMS pathway reduces OCD-like behavior. (A) Schematics showing video recordings of self-grooming in freely moving mice. (B) Schematic showing striatal localization of viral injection and fiber-optic implantation for induction of OCD-like behavior (Left). Two weeks after repeated stimulation, mice exhibited significantly increased grooming (Right; $n = 8$ mice; D1: 8 ± 1.414 , D22: 20.88 ± 2.943 ; paired t test, $P = 0.0007$), demonstrating the establishment of OCD-like repetitive behavior. (C) Strategy for optogenetic manipulation of SNC-VMS projections. Left: schematic showing striatal localization of viral injections and fiber-optic implantation for regulation of OCD-like behavior. Right: coronal sections showing the injection sites of viral injection in SNc. Scale bar, 1 mm. (D) Summarized data showing photoinhibition of SNC-VMS projections rapidly and reversibly suppressed the excessive self-grooming. Total (Left; NPHR: $n = 7$ mice; pre: 18.57 ± 2.308 ; stim: 5.286 ± 2.233 ; post: 15.43 ± 2.092 ; repeated-measure one-way ANOVA [RM one-way ANOVA] main effect: $P = 0.001$, $F(1.880, 11.28) = 14.00$; Tukey's test: pre vs. stim, $P = 0.0037$; stim vs. post, $P = 0.0003$) and normalized grooming time (Right; EYFP: $n = 6$ mice; NPHR: $n = 7$ mice; after normalization, pre: 0.9209 ± 0.1144 ; stim: 0.2478 ± 0.1047 ; post: 1.040 ± 0.1956 ; RM one-way ANOVA main effect: $P = 0.0022$, $F(1.189, 7.136) = 19.98$; Tukey's test: pre vs. stim, $P = 0.0017$; stim vs. post, $P = 0.0006$). The normalized data (N_i) were the ratio of raw data (R_i) to the averaged values of the control group. For detailed information, refer to *SI Appendix, SI Material and Methods*; all the raw data shown in *SI Appendix, Fig. S2A* in SNC-stimulated (Nphr) groups were monitored before (pre), during (stim), and after (post) stimulation. (E and F) Same as C and D except VTA-VMS projections were stimulated, scale bars in E, 1 mm. Inset: schematic of tethering habituation and stimulation paradigm to examine the role of SNC-VMS or SNC-VTA projections in regulation of OCD-like behavior for C and E. Photoinhibition of VTA-VMS projections terminals failed to affect grooming time in OCD-like mice (Left, NPHR: $n = 6$ mice; pre: 17 ± 1.915 ; stim: 14.17 ± 1.327 ; post: 14 ± 1.673 ; RM one-way ANOVA main effect: $P = 0.0038$, $F(1.540, 7.699) = 13.92$; Tukey's test: pre vs. stim, $P = 0.3247$; stim vs. post, $P = 0.9999$; Right, EYFP: $n = 6$ mice; NPHR: $n = 6$ mice; after normalization, pre: 0.9808 ± 0.1105 ; stim: 0.8019 ± 0.07512 ; post: 0.6563 ± 0.07844 ; RM one-way ANOVA main effect: $P = 0.093$, $F(1.507, 7.535) = 3.468$; Tukey's test: pre vs. stim, $P = 0.182$; stim vs. post, $P = 0.5348$; all the raw data shown in *SI Appendix, Fig. S2B*). All data are means \pm SEM. Compared between indicated groups, $**P < 0.01$, $***P < 0.001$, and ns, no significance.

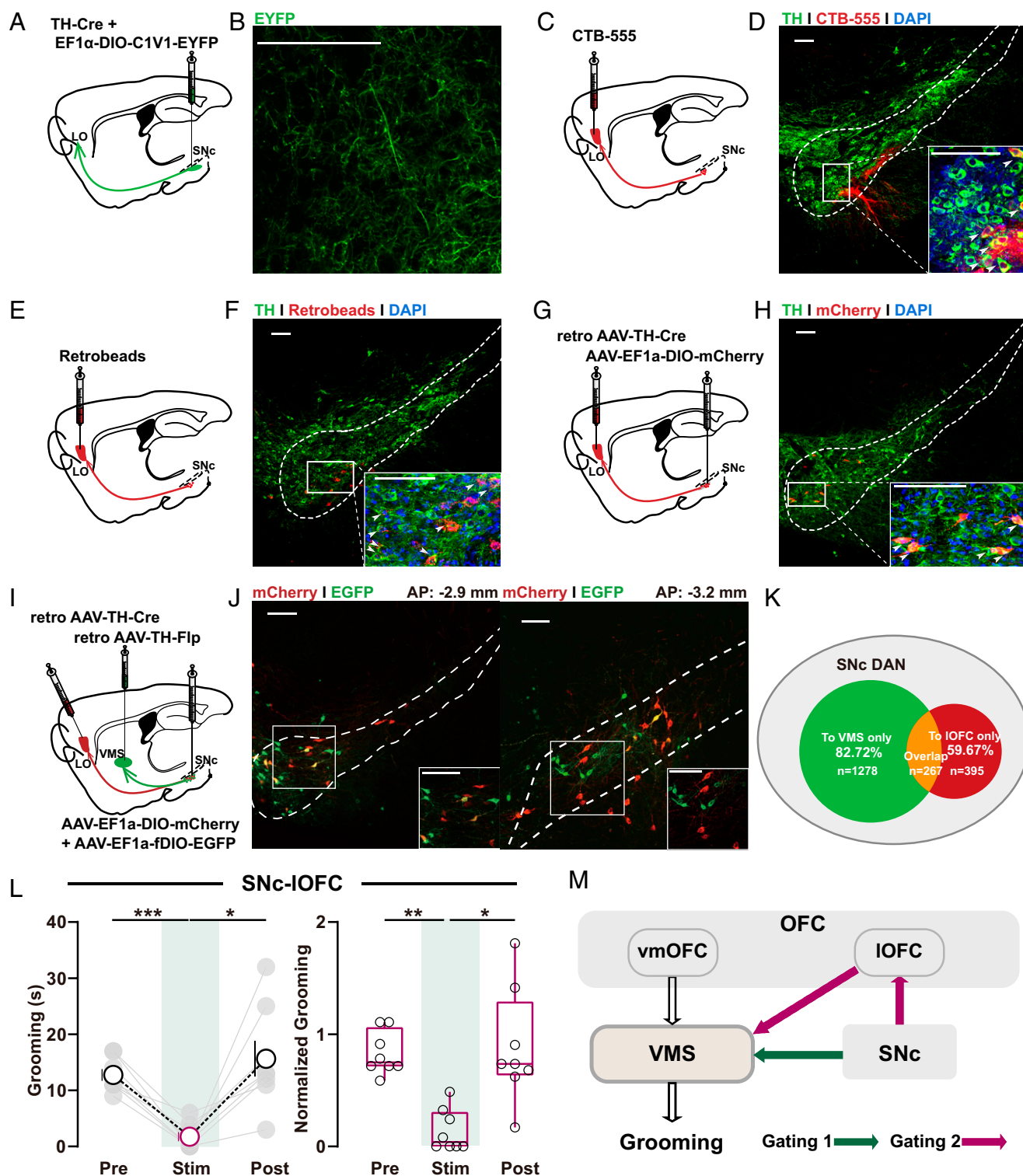


Fig. 2. SNc-IOFC excitation alleviates OCD-like behavior. (A, C, E, and G) Schematics showing localization of viral injection for anterograde (A) or retrograde tracing (C, E, and G) of SNc-IOFC (LO) projections. (B, D, F, and H) Verification of SNc-IOFC projections evidenced by anterogradely labeled axons terminals (stained with EYFP) in IOFC (B) or retrogradely labeled DAN cell bodies in SNc using retrograde tracer CTB (D), retrobeads (F), or AAV-retro-TH-Cre (H). Images at the bottom right of D, F and H are high-magnification images of the boxed area in SNc. Scale bars, 100 μ m. (I) Schematics showing localization of viral injection for retrograde tracing of SNc-IOFC and SNc-VMS projections. (J) Retrogradely traced DA neuron populations at SNc labeled by mCherry and EYFP, respectively. Inset in each panel, a high-magnification image of the boxed region. Scale bars, 100 μ m. (K) Schematics showing the relationship between different DAN populations in SNc. (L) Summarized data showing acute photoactivation of SNc-IOFC projections rapidly and reversibly suppressed the OCD-like grooming behavior. Changes in total (Left) or normalized grooming time (Right) were observed (Left, C1V1: $n = 8$ mice; pre: 12.75 ± 1.048 ; stim: 1.75 ± 0.8183 ; post: 15.63 ± 3.173 ; RM one-way ANOVA main effect: $P = 0.0035$, $F(1.301, 9.104) = 13.56$; Tukey's test: pre vs. stim, $P = 0.0003$; stim vs. post, $P = 0.0215$; Right, EYFP: $n = 6$ mice; C1V1: $n = 8$ mice; after normalization, pre: 0.8315 ± 0.0684 ; stim: 0.1419 ± 0.0664 ; post: 0.8844 ± 0.1796 ; Friedman test with Dunn's multiple comparisons test: pre vs. stim, $P = 0.0035$; stim vs. post, $P = 0.0179$; all the raw data shown in *SI Appendix, Fig. S2C*). (M) Schematic diagrams showing the long-range SNc-VMS and putative SNc-IOFC-VMS pathways for dopaminergic gating over OCD-like behavior. Compared between indicated groups, * $P < 0.05$, ** $P < 0.01$, and *** $P < 0.001$.

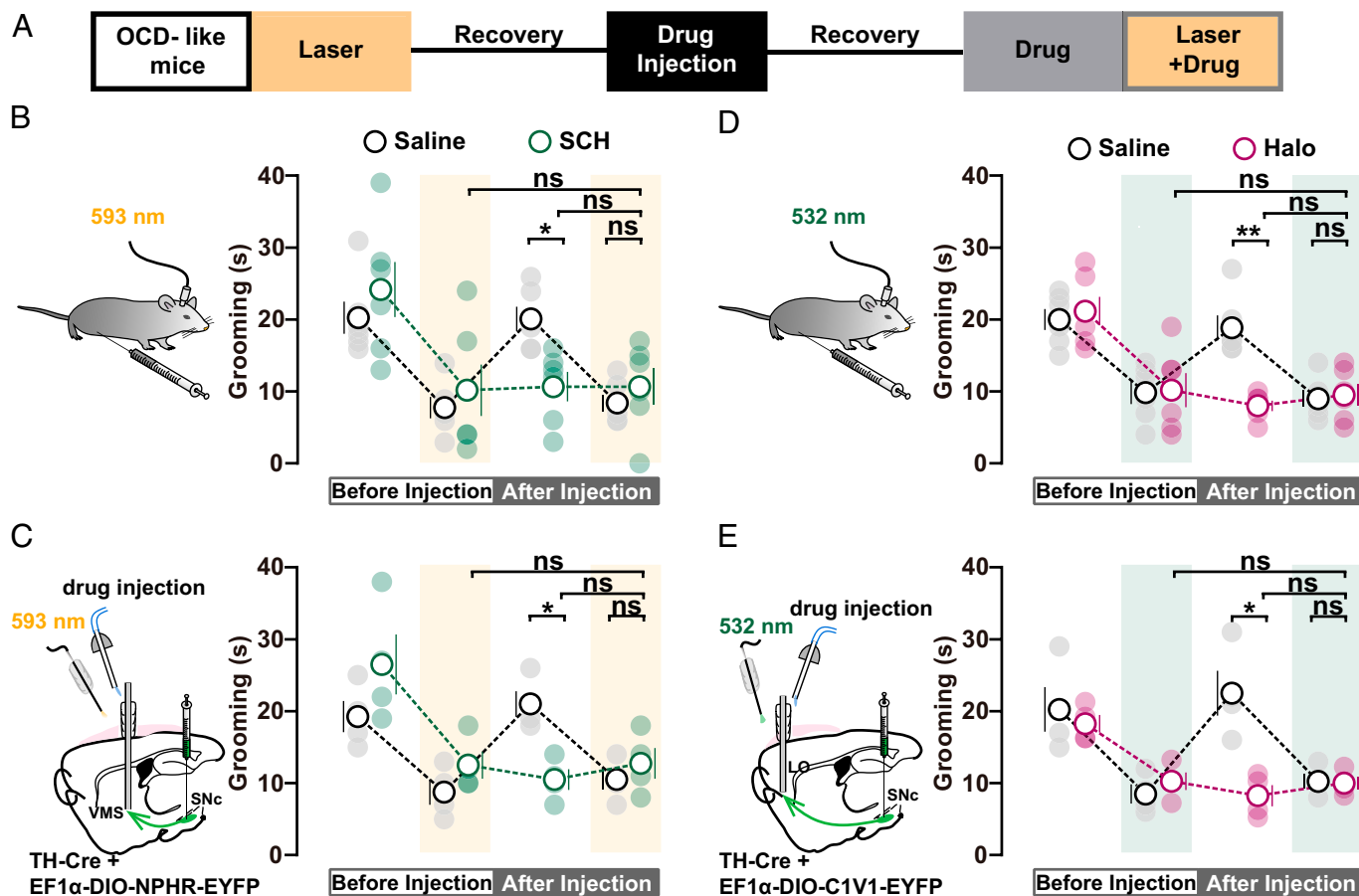


Fig. 3. Role of DA receptor subtypes in SNc-mediated gating of self-grooming. (A) Timeline of mutual occluding experiments in SNc-VMS and SNc-IOFC circuits at D22. (B) Blocking D1R occludes the effect of photoinhibition of SNc-VMS projections on self-grooming time. D1R antagonist SCH23390 (SCH) (0.05 mg/kg body weight) was applied through intraperitoneal injection (saline: $n = 6$ mice, photoinhibition: 7.833 ± 1.493 , drug: 20.17 ± 1.682 , photoinhibition plus drug: 8.5 ± 1.176 ; SCH: $n = 6$ mice, photoinhibition: 10.17 ± 3.563 , drug: 10.67 ± 2.06 , photoinhibition plus drug: 10.67 ± 2.525 ; drug: saline vs. SCH, RM two-way ANOVA with Bonferroni's test, $P = 0.0216$; photoinhibition plus drug: saline vs. SCH, RM two-way ANOVA with Bonferroni's test, $P > 0.9999$; SCH: photoinhibition vs. photoinhibition plus drug, RM two-way ANOVA with Tukey's test, $P = 0.9941$; SCH: drug vs. photoinhibition plus drug, RM two-way ANOVA with Tukey's test, $P > 0.9999$). (C) Local application of D1R antagonist SCH (150 nL) in VMS (Left) occludes the effect of photoinhibition of SNc-VMS projections on self-grooming time (saline: $n = 4$ mice, photoinhibition: 8.75 ± 1.75 , drug: 21 ± 1.78 , photoinhibition plus drug: 10.5 ± 1.443 ; SCH: $n = 4$ mice, photoinhibition: 12.5 ± 1.893 , drug: 10.5 ± 1.443 , photoinhibition plus drug: 12.75 ± 2.136 ; drug: saline vs. SCH, RM two-way ANOVA with Bonferroni's test, $P = 0.0167$; photoinhibition plus drug: saline vs. SCH, RM two-way ANOVA with Bonferroni's test, $P > 0.9999$; SCH: photoinhibition vs. photoinhibition plus drug, RM two-way ANOVA with Tukey's test, $P = 0.997$; SCH: drug vs. photoinhibition plus drug, RM two-way ANOVA with Tukey's test, $P = 0.1606$). (D and E) Same as B and C, except mutual occluding experiments were performed on SNc-IOFC projections. Intraperitoneal (0.1 mg/kg body weight; (D); saline: $n = 6$ mice, photoactivation: 9.833 ± 1.579 , drug: 18.83 ± 1.74 , photoactivation plus drug: 9 ± 1.155 ; Halo: $n = 6$ mice, photoactivation: 10.17 ± 2.372 , drug: 8 ± 0.7303 , photoactivation plus drug: 9.5 ± 1.478 ; drug: saline vs. Halo, RM two-way ANOVA with Bonferroni's test, $P = 0.0033$; photoactivation plus drug: saline vs. Halo, RM two-way ANOVA with Bonferroni's test, $P > 0.9999$; Halo: photoactivation on vs. photoactivation plus drug, RM two-way ANOVA with Tukey's test, $P = 0.9333$; Halo: drug vs. photoactivation plus drug, RM two-way ANOVA with Tukey's test, $P = 0.579$) or local application (80 nL; (E); saline: $n = 4$ mice, photoactivation: 8.5 ± 1.323 , drug: 22.5 ± 3.122 , photoactivation plus drug: 10.25 ± 1.031 ; Halo: $n = 4$ mice, photoactivation: 10 ± 1.225 , drug: 8 ± 1.472 , photoactivation plus drug: 9.75 ± 0.8539 ; drug: saline vs. Halo, RM two-way ANOVA with Bonferroni's test, $P = 0.0477$; photoactivation plus drug: saline vs. Halo, RM two-way ANOVA with Bonferroni's test, $P > 0.9999$; Halo: photoactivation on vs. photoactivation plus drug, RM two-way ANOVA with Tukey's test, $P = 0.9988$; Halo: drug vs. photoactivation plus drug, RM two-way ANOVA with Tukey's test, $P = 0.8608$) of D2R antagonist Halo occluded further effect of photoactivation of SNc-IOFC projections on self-grooming time. Compared between indicated groups, * $P < 0.05$, ** $P < 0.01$, and *** $P < 0.001$.

dual gating mechanisms in a genetically modified OCD animal model, *Sapap3* knockout (*Sapap3* KO) mice (26). Our results reveal that both photoinhibition of SNc-VMS pathway and photoactivation of SNc-IOFC pathway suppressed excessive self-grooming in *Sapap3* KO mice (SI Appendix, Fig. S8). These findings are consistent with the results in OCD-like mice and thus corroborate the current findings.

Collectively, our findings support dual gating mechanisms implemented by DANs via both striatal and cortical projections to regulate OCD-like behaviors (Fig. 2M).

Roles of Dopamine (DA) Receptors in SNc's Control over OCD-like Repetitive Behavior. Dopamine receptor antagonists have been clinically used to treat OCD symptoms, including repetitive behavior (34–36). However, it is still unknown where in the brain

the dopamine receptor takes its action and how it works to suppress OCD symptoms. To examine the roles of dopamine receptors in mediating SNc's dopaminergic gating over OCD-like behavior, we expressed eNPHR3.0 under the control of the TH promoter in SNc and implanted optic fibers in VMS in OCD-like mice. We then measured the effects of SNc-VMS inhibition on grooming behavior followed by intraperitoneal (i.p.) injection with D1R antagonist SCH23390 (SCH) (Fig. 3A). Consistent with observations in Fig. 1D, excessive self-grooming was attenuated during (but not after) photoinhibition of SNc-VMS projections. Subsequent SCH treatment via i.p. (0.05 mg/kg body weight) displayed similar attenuation of grooming time. Notably, 1 h after SCH treatment, the photoinhibition of SNc-VMS projections failed to display further effect (Fig. 3B). By contrast, an additional decrease in the time of self-grooming was observed

when SNc–VMS photoinhibition was jointly performed with i.p. injection of D2R antagonist haloperidol (Halo) (0.1 mg/kg body weight; *SI Appendix, Fig. S9A*).

To avoid SCH applied via i.p. injection yielding unspecific effects on brain regions other than VMS, we repeated the experiments by stereotactically local injecting SCH (0.1 mg/mL, 150 nL) into VMS (Fig. 3C and *SI Appendix, Fig. S1A*). Similar regulations on the time of self-grooming were observed, further pointing to the conclusion that SNc exhibits dopaminergic control over VMS local circuits via its effect on D1Rs in VMS cells. These mutual occluding experiments not only point to the involvement of D1Rs and D2Rs but also suggest that D1R and SNc–VMS share a common mechanism to gate OCD-like behavior. In other words, it's D1Rs located in SNc-projected neurons in VMS that take a crucial role in gating self-grooming.

On the other hand, similar experiments were performed to examine the role of dopamine receptors in SNc–IOFC pathway. We expressed C1V1 in DA neurons in SNc and implanted optic fibers in IOFC. We found either photoactivation of SNc–IOFC projections or treatment with D1R antagonist SCH alone suppressed self-grooming in OCD-like mice, and the joint treatment (photoactivation plus SCH) yielded further relief of repetitive behavior (*SI Appendix, Fig. S9B*). By contrast, no further effect on grooming time was observed when SNc–IOFC photoactivation and D2R antagonist Halo (0.1 mg/kg body weight) were jointly applied (Fig. 3D). These results were further confirmed by experiments with local injection of D2R antagonists Halo (0.2 mg/mL, 80 nL) into IOFC (Fig. 3E and *SI Appendix, Fig. S1B*), indicating D2Rs in SNc-targeted IOFC are involved in gating of self-grooming. Importantly, the role of DA receptors in gating self-grooming in the two pathways was validated in *Sapap3* KO mice (*SI Appendix, Fig. S10 A and B*).

Taken together, these results indicate distinct dopaminergic signaling profiles in striatal or cortical dopaminergic projections in the regulation of grooming.

Distinct VMS Microcircuits Related to Self-Grooming Dysregulation.

To understand the detailed modulation of VMS microcircuits underlying dopaminergic modulation of grooming behavior, we first examine how VMS microcircuits were changed during self-grooming dysregulation in OCD-like mice. The striatum is a core region that processes the output information of behavior in the CSTC circuit. There are various types of neurons in the striatum, including medium spiny neurons (MSNs) and interneurons, and both the activity of these neurons and their connections play a crucial role in information processing. Before we start to dissect how VMS microcircuits were changed during self-grooming dysregulation in OCD-like mice, we need to first identify and differentiate each specific type of neuron under physiological conditions. For this purpose, we employed the “opto-tagging” technique (37, 38) and targeted different cell types by injecting Cre-inducible AAV expressing photoactivated opsins into the VMS of the Cre mouse for single-unit spike recording and optogenetic activation. We used parvalbumin (PV)-Cre, somatostatin (SOM)-Cre, and choline acetyltransferase (ChAT)-Cre mice for cell type-specific expression of fluorescent proteins and photoactivated opsins [ChR2-E123T accelerated (ChETA) for PV-Cre, ChR2 for SOM- and ChAT-Cre]. Recordings were made in freely moving mice by implanting optrodes consisting of 32-channel movable electrode bundles coupled to a fiber-optic cannula placed just above the VMS (39) (*SI Appendix, Fig. S1C*). Different frequency laser-pulse trains (10 or 40 Hz, 5 ms per pulse) were applied intermittently (Fig. 4A). Single units exhibiting reliable laser-evoked spiking at short latencies were

obtained (Fig. 4A–C and *SI Appendix, Fig. S11A*). Then, three waveform parameters from all these recorded neurons, length of peak 1 to peak 2, the valley full width at half-maximum (FWHM), and the spike asymmetry (*SI Appendix, Fig. S11B*), were plotted. These plottings yielded three clusters that could be clearly separated by a clustering algorithm and were identified as putative PV, SOM, and ChAT interneurons in respective Cre mice (Fig. 4D and *SI Appendix, Fig. S11 C–E*). To further classify these feature profiles, we used principal-component analysis (PCA) followed by unsupervised clustering. This yielded three clusters of neurons that were separated according to PC 1 and PC 2 (Fig. 4E). MSNs displayed characteristic features in a single-unit waveform with wide spikes (>0.55 ms trough-to-peak duration) (38) and low firing rates (<2 Hz) (40). In sum, these results obtained under physiological conditions enabled us to identify and differentiate each putative cell type based on their waveform features.

We next investigated how these identified neurons in VMS microcircuits changed in OCD-like mice (Fig. 4F and *SI Appendix, Fig. S1D*). Because the waveforms of spontaneous and optogenetically induced spiking matched perfectly (Fig. 4C), in the following experiments, we identified each putative cell type according to the waveforms of spontaneous spiking, just as done in previous studies (37, 38). We found that spike firing of most MSNs (13 in 16 cells) and PV cells (14 in 27 cells; termed as PV I) were increased after stimulation of vmOFC–VMS projections (Fig. 4G and H). Notably, a small subset of PV cells (11 in 27 cells; termed PV II) displayed reduced activity (Fig. 4I). In contrast, the firing of the SOM population was decreased (9 in 12 cells; Fig. 4J) and firing of the ChAT population was unchanged during daily stimulation (8 in 10 cells; Fig. 4K). The averaged baseline firing rate of the two PV populations seems quite different, at 5–10 Hz and 20–30 Hz, respectively, indicating distinct baseline activity in the two populations of PV neurons. Interestingly, at the end of the induction of OCD-like behavior, the firing rate of the two PV populations reaches similar levels (around 15 Hz; Fig. 4H and I).

To further determine whether the down- or upregulation of distinct interneuron populations is associated to constitute striatal microcircuits underlying OCD-like repetitive behavior, we took advantage of the principle that monosynaptic connections were associated with precisely timed spiking relationships at short (<5 ms) latency offsets between two connected neurons (41). Cross-correlograms of spike trains achieved by examining counts of co-occurrences of spiking between the neuron pairs at various differential time lags (42) can reveal putative synaptic connections between them. Our results suggest the sequences for firing alterations among different cell subtypes, i.e., PV I cells preceded SOM cells (Fig. 4L) and SOM cells preceded MSNs (Fig. 4M), according to the sequences for firing alterations. Especially, PV I neurons with increased activity under the OCD state (Fig. 4H) subsequently inhibited SOM that directly connected with them (Fig. 4L) and caused reduced activities of SOM neurons (Fig. 4J), which in turn disinhibited MSNs (Fig. 4G and M). In addition, according to the sequences for firing alterations, PV II cells with reduced activity (Fig. 4I) were observed directly preceding MSNs (Fig. 4N) and subsequently disinhibited MSNs (Fig. 4G). These results indicate that PV populations with different activity changes may take part in distinct VMS microcircuits to contribute to self-grooming dysregulation.

Dual Gating Effects on OCD-like Repetitive Behavior in VMS.

We next examine how the two SNc-mediated long-range circuits interact with VMS microcircuits to regulate self-grooming in OCD-like mice. We specifically expressed eNPHR3.0 in

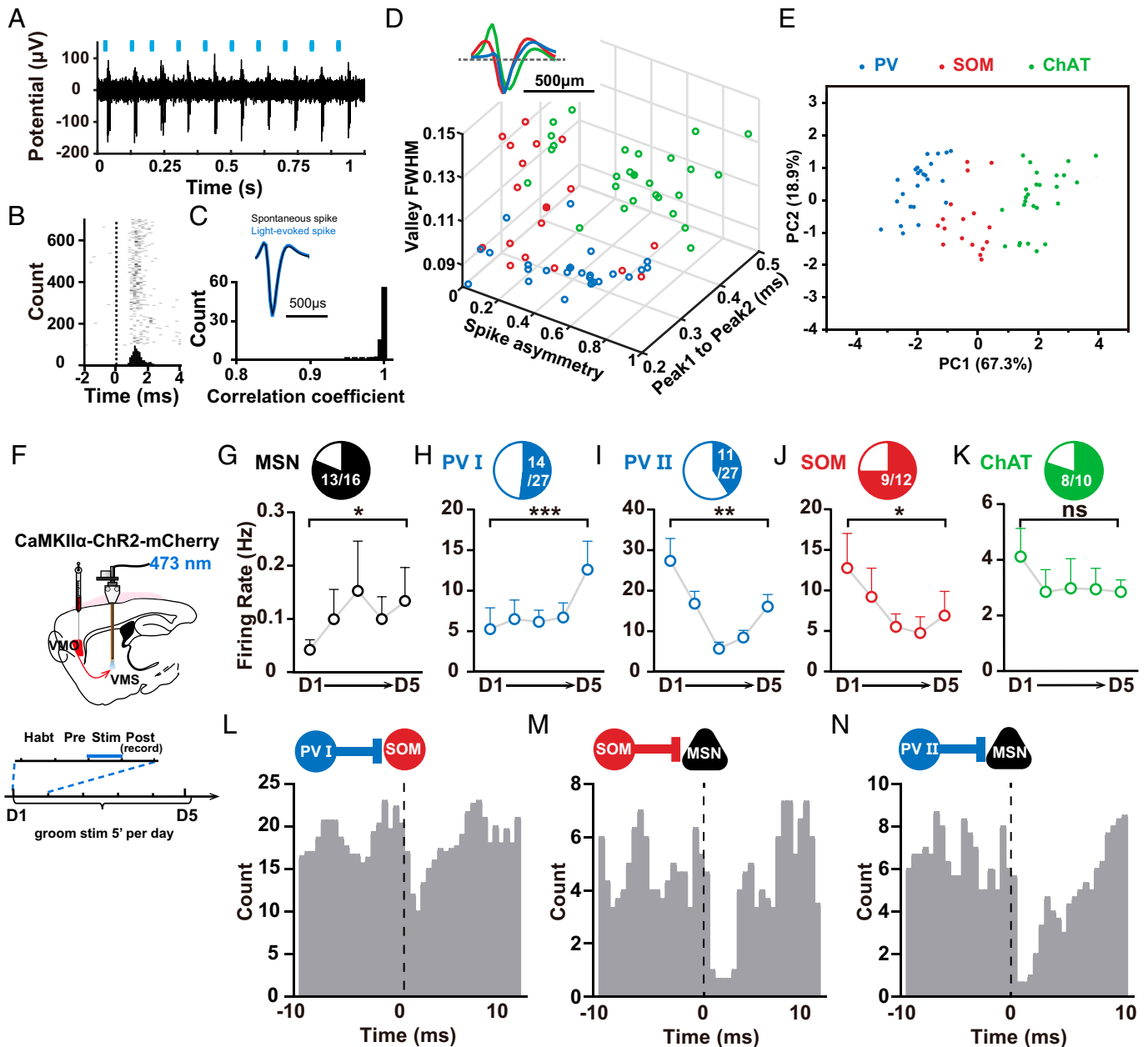


Fig. 4. VMS microcircuits related to self-grooming dysregulation in OCD-like mice. (A) Representative recording of laser-evoked spiking in SOM-ChR2 mice. Blue lines represent laser pulses (5 ms, 10 Hz). (B) Raster plot and peri-stimulus time histogram (bin size, 0.5 ms) for laser-evoked spikes of the same ChR2-tagged SOM neuron shown in A. Dashed line, laser onset time. (C) Waveform comparison between light-evoked and spontaneous spikes. (D) Top, averaged waveforms of light-evoked spikes (blue) and spontaneous spikes (black) of an example neuron. Bottom, distribution of correlation coefficient between light-evoked and spontaneous spike waveforms for all 67 optogenetically identified neurons at VMS. (E) Separation of striatal interneuron subtypes based on physiological properties for optogenetically identified neurons. The parameters of mean waveforms for each neuron were plotted against each other, revealing three clear clusters corresponding to PV, SOM, and ChAT interneurons (SI Appendix, Fig. S5 B–E). (F) Classification of neurons based on PC 1 and PC 2 after PCA. (G) Schematics showing localization of viral injections and optrode recordings. (G–K) Activity changes in optogenetically identified striatal neuron subtypes during induction of OCD-like behavior for 5 consecutive days ((G) $n = 16$ neurons, D1: 0.0421 ± 0.01867 , D5: 0.1338 ± 0.0627 , D1 vs. D5, Wilcoxon signed rank test, $P = 0.0498$; (H) $n = 14$ neurons, D1: 5.25 ± 2.64 , D5: 12.59 ± 3.508 , D1 vs. D5, Wilcoxon signed rank test, $P = 0.0001$; (I) $n = 11$ neurons, D1: 27.36 ± 5.516 , D5: 16.06 ± 2.992 , D1 vs. D5, Wilcoxon signed rank test, $P = 0.002$; (J) $n = 12$ neurons, D1: 12.76 ± 4.257 , D5: 6.898 ± 2.988 , D1 vs. D5, Wilcoxon signed rank test, $P = 0.0391$; (K) $n = 10$ neurons, D1: 4.112 ± 1.016 , D5: 2.843 ± 0.4317 , D1 vs. D5, paired t test, $P = 0.1324$). (L–N) Putative synaptic connections revealed by sequences of firing alterations among different neuron subtypes. Monosynaptic connections were associated with precisely timed spiking relationships at short (<5 ms) latency offsets between two connected neurons (41). Cross-correlogram of spike trains was achieved by examining counts of co-occurrences of spiking between the neuron pairs at various differential time lags. (L) PV I-SOM neuron pair; (M) SOM-MSN neuron pair; (N) PV II-MSN neuron pair. PV I neurons with increased activity under OCD state subsequently inhibit SOM that directly connects with them and caused reduced activities of SOM neurons, which in turn disinhibited MSNs. In addition, according to the sequences for firing alterations, PV II cells with reduced activity were observed directly preceding MSNs and subsequently disinhibited MSNs. Compared between indicated groups, $*P < 0.05$, $**P < 0.01$, and $***P < 0.001$.

DANs in SNc and implanted optrodes in VMS to photoinhibit SNc–VMS axon terminals (~5 mW, 5 min) and to record activity changes in different types of striatal neurons in freely moving OCD-like mice. We found that the activity changes in optogenetically identified cell subtypes, including increased

activity in PV I cells and MSNs, as well as reduced activity in SOM cells, were reversed during the SNc–VMS terminal photoinhibition in OCD-like mice (Fig. 5 A–C). These observations indicate that SNc can gate OCD-like self-grooming by toning down its dopaminergic control over VMS microcircuits.

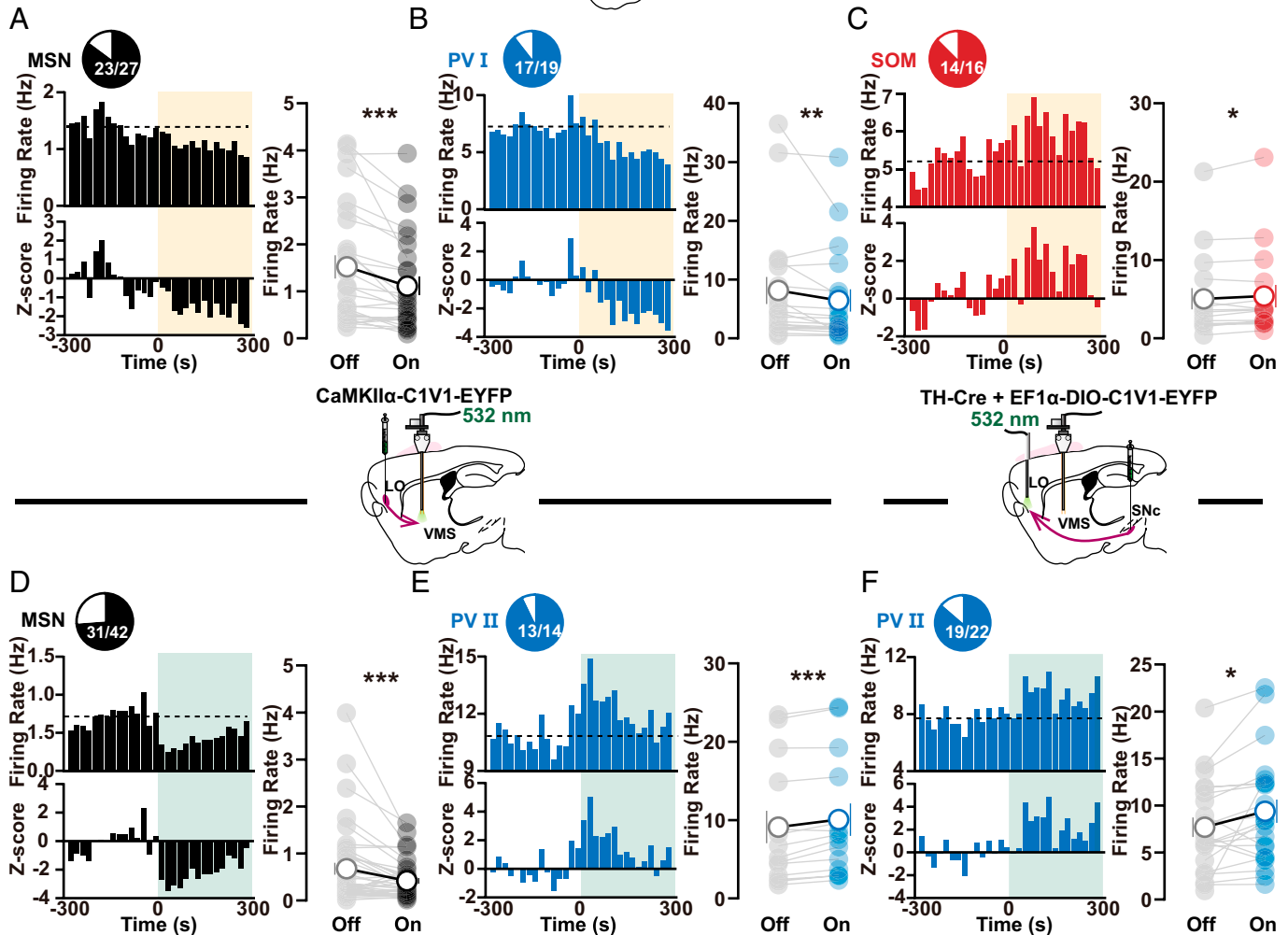
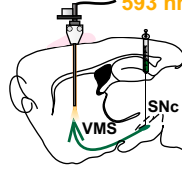


Fig. 5. Distinct activity changes in VMS microcircuits mediated by two SNc-mediated pathways. (A–C) Activity changes in optogenetically identified striatal MSN ((A) $n = 27$ neurons, off: 1.521 ± 0.2472 , on: 1.11 ± 0.1953 , off vs. on, Wilcoxon signed rank test, $P < 0.0001$), PV I ((B) $n = 19$ neurons, off: 8.135 ± 2.301 , on: 6.448 ± 1.893 , off vs. on, Wilcoxon signed rank test, $P = 0.0175$) cell subtypes during photoinhibition of SNc–VMS axon terminals in OCD-like mice. Statistical plotting (Right in each panel) shows decreased firing in MSNs and PV I cells, as well as increased firing in SOM cells (Wilcoxon signed rank test). (D–F) Same as A–C except IOFC–VMS (D and E) ($n = 42$ neurons, off: 0.6757 ± 0.1271 , on: 0.4162 ± 0.06156 , off vs. on, Wilcoxon signed rank test, $P = 0.0003$; (E) $n = 14$ neurons, off: 9.116 ± 2.07 , on: 10.06 ± 2.064 , off vs. on, paired t test, $P = 0.0002$) or SNc–IOFC (F) ($n = 22$ neurons, off: 7.695 ± 1.035 , on: 9.397 ± 1.238 , off vs. on, paired t test, $P = 0.0214$) projections were photoactivated. In contrast to the results in A–C, increased firing was observed in PV II cells (Wilcoxon signed rank test or paired t test). Compared between indicated groups, * $P < 0.05$, ** $P < 0.01$, and *** $P < 0.001$.

In a separate set of experiments, we examined how SNc–IOFC pathway would affect VMS local circuits during gating of self-grooming. We expressed C1V1 under the control of the TH promoter in ventral SNc and implanted optic fiber into IOFC to stimulate SNc axon terminals in this subregion. Recordings were made with implanted multichannel tetrode in VMS in freely moving OCD-like mice. During optogenetic stimulation of SNc axon terminals in IOFC, the decreased activity in PV II neurons was reversed (19 in 22 cells; Fig. 5F).

Given the previous finding that optogenetic stimulation of IOFC–VMS inputs restores both OCD-like repetitive behavior and impaired fast spiking neuron in striatal microcircuits (26), our results point to the possibility that photoactivation of the SNc–IOFC pathway selectively interacts with downstream

IOFC–VMS pathway, i.e., IOFC functions as a relay station to implement SNc's control over VMS. To test this possibility, we next investigated how stimulating glutamatergic IOFC–VMS projections affect VMS microcircuits. We expressed C1V1 in glutamatergic neurons in IOFC and implanted the optrode just above left VMS for axon terminal stimulation and neuron activity detection. We then delivered 532-nm optogenetic stimulations (~ 5 mW, 10 ms, 20 Hz) at VMS and detected decreased firing in MSNs (31 in 42 cells; Fig. 5D) and increased firing in PV II neurons (13 in 14 cells; Fig. 5E) during stimulation, similar to the observations exhibited by activating SNc–IOFC projections (Fig. 5F). No such changes in spike firing were observed in SOM cells during SNc–IOFC or IOFC–VMS excitation (SI Appendix, Fig. S12 A and B). Moreover, direct glutamatergic

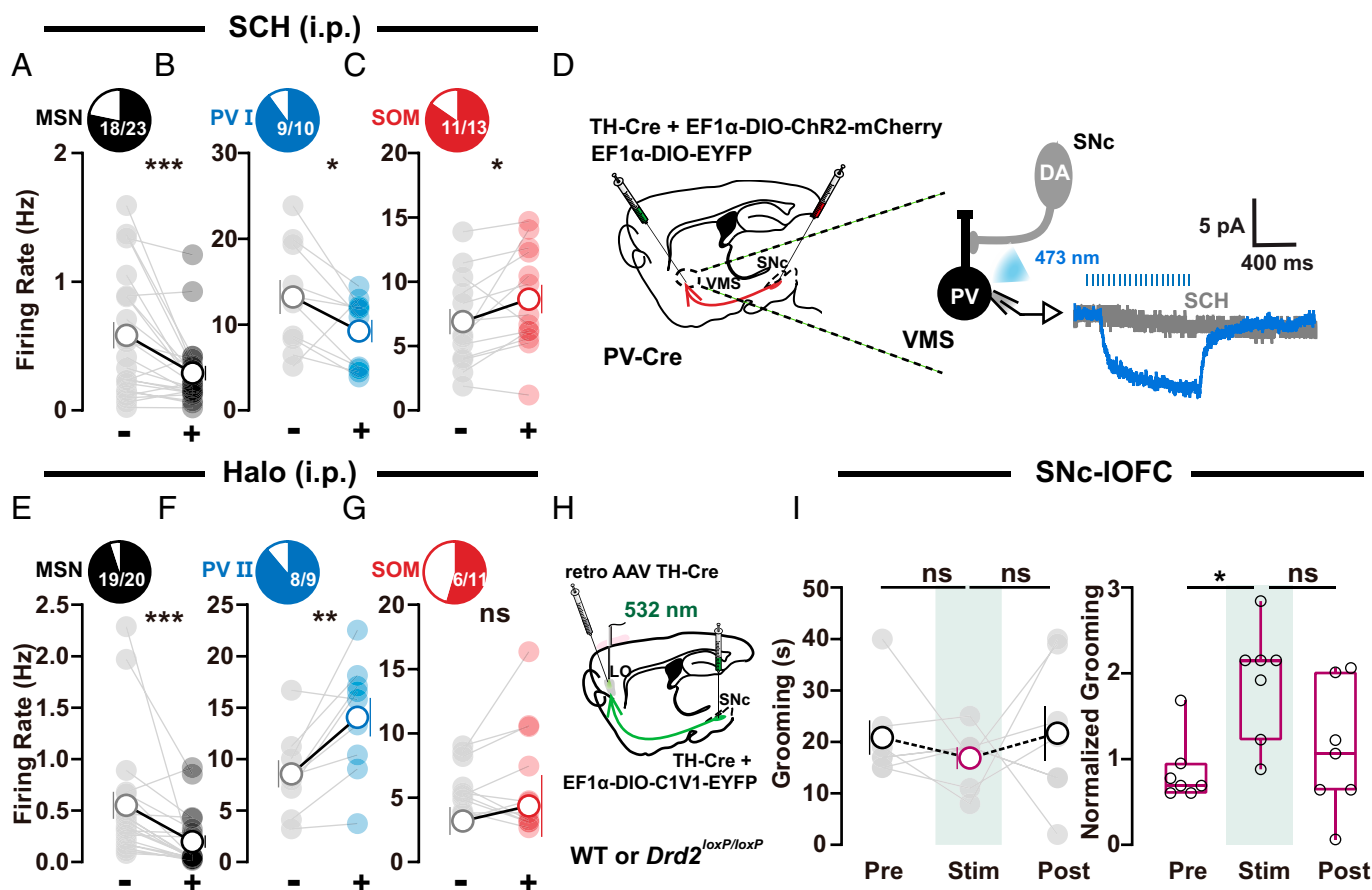


Fig. 6. D1R and D2R antagonists differentially regulate VMS microcircuits. (A–C) Activity changes in MSNs, PV I, and SOM neurons in VMS after treatment with D1 receptor blocker SCH ((A) $n = 23$ neurons, $-: 0.5839 \pm 0.1027$, $+: 0.2899 \pm 0.05704$, $-$ vs. $+$, Wilcoxon signed rank test, $P = 0.0009$; (B) $n = 10$ neurons, $-: 13.22 \pm 1.982$, $+: 9.257 \pm 1.31$, $-$ vs. $+$, Wilcoxon signed rank test, $P = 0.0488$; (C) $n = 13$ neurons, $-: 6.896 \pm 0.9854$, $+: 8.651 \pm 1.114$, $-$ vs. $+$, paired t test, $P = 0.0445$). (D) Optogenetic stimulation of SNc axon terminals in VMS elicited a slow deflection that was totally abolished by D1R antagonist SCH (10 μ M). (E–G) Activity changes in MSNs, PV II, and SOM neurons in VMS after treatment with D2 receptor blocker Halo ((E) $n = 20$ neurons, $-: 0.5512 \pm 0.1305$, $+: 0.1988 \pm 0.06089$, $-$ vs. $+$, Wilcoxon signed rank test, $P < 0.0001$; (F) $n = 9$ neurons, $-: 8.569 \pm 1.323$, $+: 14.07 \pm 1.872$, $-$ vs. $+$, paired t test, $P = 0.0059$; (G) $n = 11$ neurons, $-: 5.758 \pm 0.5968$, $+: 6.398 \pm 1.322$, $-$ vs. $+$, Wilcoxon signed rank test, $P = 0.7002$). (H) Schematic showing localization of viral (retro AAV TH-Cre) injections for selective knockout of D2 autoreceptors in SNc DA neurons and fiber-optic implantation for stimulation of SNc–IOFC projections. (I) Summarized data showing that, in OCD-like mice with D2Rs knockout in SNc DA neurons (H), SNc–IOFC excitation failed to exert any effect on grooming time. Changes in total (Left, *Drd2^{loxP/loxP}*; $n = 7$ mice; pre: 20.86 ± 3.355 ; stim: 16.86 ± 2.143 ; post: 21.71 ± 5.299 ; RM one-way ANOVA main effect: $P = 0.5694$, $F(1.319, 7.912) = 0.4605$; Tukey's test: pre vs. stim, $P = 0.5622$; stim vs. post, $P = 0.7766$) or normalized grooming time (Right, wild type [WT]; $n = 6$ mice, *Drd2^{loxP/loxP}*; $n = 7$ mice; after normalization, pre: 0.9003 ± 0.1448 ; stim: 1.945 ± 0.2473 ; post: 1.143 ± 0.2789 ; RM one-way ANOVA main effect: $P = 0.0661$, $F(1.095, 6.572) = 4.761$; Tukey's test: pre vs. stim, $P = 0.019$; stim vs. post, $P = 0.3016$). Significance between pre and stim (Right) was caused by data normalization, and the normalized data (N) was the ratio of raw data (R_i) to the averaged values of the control group. For detailed information, refer to *SI Appendix, SI Material and Methods*; all the raw data are shown in *SI Appendix, Fig. S2D*. Compared between indicated groups, * $P < 0.05$, ** $P < 0.01$, and *** $P < 0.001$.

monosynaptic connections between pyramidal neurons from IOFC and PV neurons in VMS were confirmed (*SI Appendix, Fig. S13 A and B*). These results suggest a long-range SNc–IOFC–VMS circuit participates in dopaminergic regulation of the VMS microcircuit.

Using AAV-mediated anterograde transsynaptic tagging of PV neurons in VMS (43, 44), we further demonstrated that the PV neurons with different activity changes (PV I and PV II neurons) largely belong to two distinct populations (*SI Appendix, Fig. S14*).

To prove the causality of VMS microcircuits in OCD-like behavior, we selectively manipulated each cell type in VMS during grooming behaviors. Our results show that optogenetic deactivation of PV I cells or activation of SOM cells in VMS suppressed grooming time in OCD-like mice (*SI Appendix, Fig. S15 A–D*). On the other hand, optogenetic activation of PV II cells reduced grooming time (*SI Appendix, Fig. S15 E and F*).

Collectively, our results indicate that SNc–VMS and SNc–IOFC dopaminergic projections differentially modulate grooming behaviors and striatal microcircuit function. Specifically, the activity of the SNc–VMS pathway promotes grooming via D1Rs,

whereas the activity of the SNc–IOFC pathway suppresses grooming via D2Rs.

D1R and D2R Antagonists Differentially Regulate VMS Microcircuits.

We next examined the role of VMS D1Rs and IOFC D2Rs in the regulation of VMS microcircuits that are related to self-grooming dysregulation in OCD-like mice. Blocking D1Rs with SCH via i.p. (0.05 mg/kg body weight) reversed activity changes in different cell types in OCD-like mice by suppressing the firing rate of MSNs (18 in 23 cells; Fig. 6A) and PV I neurons (9 in 10 cells; Fig. 6B) and elevating firing rate of SOM neurons (10 in 13 cells; Fig. 6C). To further examine whether SNc DANs can interact with PV cells in VMS via D1Rs, we expressed ChR2 in SNc DANs under the control of TH promoter and performed whole-cell patch recordings on EYFP-tagged PV cells in acute VMS slices. Single-pulse optogenetic stimulation (4 ms) of SNc axon terminals in VMS did not elicit fast postsynaptic currents in PV cells, indicating no corelease of glutamate or gamma-aminobutyric acid upon stimulations. However, we do detect a slow deflection occurring at about 100 ms after stimulations

(4 ms, 20 Hz for 1 s; Fig. 6D). Notably, this slow component could be abolished by perfusing slices with D1R antagonist SCH (10 μ M), suggesting stimulation of SNc inputs can directly activate slow responses mediated by D1Rs on PV cells in VMS. By contrast, the experiments performed in a separate cohort of OCD-like mice showing blocking D2Rs with Halo (0.1 mg/kg body weight) suppressed the activity of MSNs (19 in 20 cells; Fig. 6E) and increased the activity of PV II neurons (eight in nine cells; Fig. 6F). Importantly, risperidone (0.25 mg/kg), a drug possessing antagonistic action on D2Rs and is currently used to treat neuropsychiatric diseases with repetitive behaviors, including OCD and autism, displays similar effect on the activity of MSNs (14 in 18 cells) and PV II (9 in 10 cells) (*SI Appendix, Fig. S16*).

To examine the role of D2R in IOFC in the regulation of OCD-like behavior, we knocked out D2 autoreceptors in SNc DANs projecting to IOFC by injecting retro AAV TH-Cre, a kind of AAV tool with retrograde functionality (45), into IOFC of *Drd2^{loxP/loxP}* mice, which possess loxP sites flanking exon 2 of the dopamine receptor D2 (*Drd2*) gene (Fig. 6H). When injected into the IOFC of the *Drd2^{loxP/loxP}* mice, retro AAV viral particles traveled retrogradely toward the DANs under the control of TH promoter and KO D2 autoreceptors without effect on postsynaptic D2R of nondopaminergic neurons. Notably, in OCD-like mice with D2 autoreceptors KO in IOFC-projecting SNc DANs, SNc–IOFC excitation failed to exert any effect on grooming time (Fig. 6I and *SI Appendix, Fig. S2*).

Taken together, our results point to the conclusion that long-range SNc–VMS and SNc–IOFC circuits mediate SNc dopaminergic regulation of self-grooming through their actions on postsynaptic D1R in VMS PV cells and presynaptic D2Rs in IOFC-targeting DANs, respectively.

Discussion

The present study suggests that midbrain DANs from SNc orchestrate grooming behavior through both cortical and striatal projections, which may imply clinical treatments for OCD. In particular, the SNc–IOFC projection, as well as its function, have not been previously reported. D1R on PV neurons in VMS and D2R on axon terminals of SNc–IOFC projections are implicated in the gating of self-grooming through post- and presynaptic mechanisms, respectively (*SI Appendix, Fig. S17*). The dual gating via midbrain DA neurons for grooming behavior may serve as an endogenous homeostatic mechanism to prevent overgrooming. The cortical modulation further allows for therapeutic targeting of OCD symptoms with noninvasive brain stimulation approach.

Grooming behavior is considered one stereotypical behavior implicated in OCD, which is modulated by CSTC circuit dysfunction (46–48). For instance, the striatum regulates the execution of sequential patterns of grooming behavior (49, 50). Deep-brain stimulation of the striatum that reduces grooming behavior is associated with altered SNc DANs activities (51, 52). Our present results supported the normalization of dopaminergic activities in regulating grooming and rationalized the brain-stimulation therapy against OCD. In clinical practice, around half of OCD patients failed to exhibit a response to serotonin-reuptake inhibitors treatment (53); however, they were responding to DA antagonists (54, 55). Whether dopaminergic alteration is universal in clinical OCD patients remains to be investigated in future studies.

Several other issues needed to be further clarified. Firstly, grooming is a representative but nonexclusive phenotype for

OCD-like behaviors (56). Recent studies employed reversal learning, or compulsive checking behavior may offer improved ecological value and translational insights for OCD patients with different symptoms (57–60). The potential importance of dopaminergic signaling in these behaviors is to be determined. Secondly, whether imbalance or competence between cortical and striatal dopaminergic activities results in OCD-like behavior remains unelucidated. It will be important to investigate the neuronal activities of DANs projecting to VMS and IOFC during grooming. Thirdly, the dynamics of excitation–inhibition balance within VMS microcircuits during the generation of OCD-like behavior need to be further addressed. Fourthly, previous studies indicate that VTA DANs mainly project to the NAc (61, 62). The lack of an effect in manipulating the VTA–VMS projections (Fig. 1F) could be due to the fact that these projections are sparse or weak. In addition, as the SNc DANs in the two pathways could be only partially labeled (Fig. 2 I–K), we should not exclude the possibility that the overlap rate of the two DAN populations was underestimated.

In sum, the results indicate the hub role of SNc to orchestrate local and long-range neural circuits and exploit dual gating of pathological repetitive behaviors through distinct dopaminergic signaling. These data hint at a dopamine-integrated model of pathophysiology and treatment strategies for OCD-like behavior.

Materials and Methods

Refer to *SI Appendix, SI Material and Methods* for mouse strains information, various virus preparation and injection, surgical procedures, normalized behavioral data calculating, mobility and anxiety assays, retrograde and anterograde labeling strategy, immunofluorescence, drug application, optogenetic identification of striatal neurons, and brain slices preparation for electrophysiological recordings in vitro.

Animals. Mice were housed in a 12-h (h) light–dark cycle (lights on at 07:00 AM and off at 07:00 PM) with ad libitum access to laboratory food pellets and water. All experiments were performed in male mice (strain information provided in *SI Appendix, SI Material and Methods*). All animals were older than 2 mo at the start of experiments. All experimental protocols were conducted under the regulations of the Experimental Animal Ethics Committee of Southeast University.

Optogenetic Manipulation. After allowing sufficient time for the viral expression and surgical recovery (for detailed methods, refer to *SI Appendix, SI Material and Methods*), optogenetic manipulations were performed, using a 200 μ m, 0.22 numerical aperture fiber-optic patch cord to deliver light to a specific brain area. The laser intensities of the fiber tip were adjusted to \sim 5 mW for optogenetic manipulation.

Behavioral Assays. Mice between 12 and 16 wk (*Sapap3* KO mice between 12 and 30 wk) were habituated to the experimenter and the open-field box (40 cm \times 40 cm \times 40.5 cm) every day at the same time for 5 consecutive days before the experiment. We placed a camera above the chamber to record the behavior during each trial. Following tethering, mice were placed in an open-field box for data collection. Animal behavior was recorded using Any-maze (Stoelting), beginning after 5 min of habituation to a new cage. Grooming behavior in all trials was recorded by a camera and hand scored blindly. For detailed information for normalized behavioral data calculating and mobility and anxiety assays, refer to *SI Appendix, SI Material and Methods*.

Anatomical Verification. Mice were perfused with 4% paraformaldehyde in phosphate-buffered saline (PBS), then dissected brains were postfixed overnight and equilibrated in 40% sucrose in PBS. Next, we sliced them into 35- μ m coronal sections using a freezing microtome (CM1950, Leica). To verify the dopaminergic projection from SNc to IOFC, we used the experimental protocol mentioned in *SI Appendix, SI Material and Methods* for immunofluorescence detection of

TH+ cells in SNc. Well-prepared slices were stained with DAPI (0100-20, SouthernBiotech) and examined by confocal microscope (LSM900, Zeiss).

Optrode Recordings. Using a 32-channel optrode (39) and a multichannel recording system (Plexon Inc.), we recorded the neural activity of target brain regions in vivo. Four platinum-iridium wires (California Fine Wire) were twisted together as a tetrode and then electroplated with gold solution (Plexon Inc.) to an impedance between 150 and 300 k Ω . For optogenetic effect investigation, an optic fiber was inserted \sim 0.2 mm above the tetrode tip. Implantation of optrode was conducted as mentioned above, followed by 2 wk of recovery before recording. Spiking signals were filtered at 0.25–5 kHz and then digitized at a sampling rate of 40 kHz.

Spike Sorting and Data Analysis. The spiking data were sorted using Offline Sorter V4 (Plexon Inc.), described previously (37). Signals were thresholded at $3\times$ SD to isolate spikes, and spikes were clustered based on PCA (39, 63). Spiking activities were subsequently quantified by frequencies and Z score (63).

Electrophysiological Recordings In Vitro in Brain Slices. Whole-cell, voltage-clamp recordings were made from EYFP-stained PV neurons in well-prepared brain slices (details are in *SI Appendix, SI Material and Methods*) using an Axopatch 700B amplifier (Molecular Devices) and acquired at 10 kHz and filtered to 2 kHz. To photoactivate SNc (Fig. 6D) axons expressing ChR2 in VMS, trains of 470 nm at 20 Hz with 4-ms pulse width light pulses were applied via a light-emitting diode light source (Thorlabs). Slow inhibitory postsynaptic currents of EYFP-stained PV neurons in VMS were recorded. SCH (10 μ M, Abcam, ab120597) was added to block inhibitory currents mediated by D1Rs. To photoactivate IOFC (*SI Appendix, Fig. S13*) axons expressing ChR2 in VMS, a single

pulse was applied and excitatory postsynaptic currents of PV neurons were recorded. NBQX (10 μ M, Sigma-Aldrich, N171) was added to block light-evoked excitatory postsynaptic potentials.

Statistics. All our sample sizes were similar to those generally employed in the field. Data are presented as mean \pm SEM. Statistical analysis was done using GraphPad Prism version 8 (GraphPad Software). First, we used the D'Agostino and Pearson test (for $n > 7$) or Shapiro-Wilk test (for $n < 8$) to examine the normality of the data distribution. For samples that passed the normality test, statistical significance was calculated using a two-tailed unpaired t test and paired t test for nonpaired and paired parameters comparison, respectively, or by repeated-measure one-way and two-way ANOVA with Tukey's and Bonferroni's multiple comparisons test. For samples that did not pass normal distribution, statistical significance was calculated using the nonparametric Mann-Whitney test and Wilcoxon signed rank test, respectively, or the Friedman test with Dunn's multiple comparisons test.

Data, Materials, and Software Availability. All data are included in the manuscript and/or *SI Appendix*.

ACKNOWLEDGMENTS. We thank Dr. Huimeng Lei, Dr. Peng Cao, Dr. Fuqiang Xu, Dr. Chunjie Zhao, and Dr. Yingmei Lu for their donation of transgenic mice and technical support. This research was supported by grants to W.Lu. from the National Natural Science Foundation of China (31730107, 31970959, and 31671056) and the Ministry of Science and Technology (2021ZD0203502). We thank all members of the Lu lab for their discussion and support. We also thank Ms. He Yang for help in editing the manuscript.

1. M. E. Hirschtritt, M. H. Bloch, C. A. Mathews, Obsessive-compulsive disorder: Advances in diagnosis and treatment. *JAMA* **317**, 1358–1367 (2017).
2. T. W. Robbins, M. M. Vaghi, P. Banca, Obsessive-compulsive disorder: Puzzles and prospects. *Neuron* **102**, 27–47 (2019).
3. R. Kim *et al.*, Cell-type-specific *Shank2* deletion in mice leads to differential synaptic and behavioral phenotypes. *J. Neurosci.* **38**, 4076–4092 (2018).
4. K. K. Ade *et al.*, Increased metabotropic glutamate receptor 5 signaling underlies obsessive-compulsive disorder-like behavioral and striatal circuit abnormalities in mice. *Biol. Psychiatry* **80**, 522–533 (2016).
5. V. Tatavarthy *et al.*, Autism-associated *Shank3* is essential for homeostatic compensation in rodent V1. *Neuron* **106**, 769–777.e4 (2020).
6. X. Yu *et al.*, Reducing astrocyte calcium signaling in vivo alters striatal microcircuits and causes repetitive behavior. *Neuron* **99**, 1170–1187.e9 (2018).
7. J. Peça *et al.*, *Shank3* mutant mice display autistic-like behaviours and striatal dysfunction. *Nature* **472**, 437–442 (2011).
8. Y. Mei *et al.*, Adult restoration of *Shank3* expression rescues selective autistic-like phenotypes. *Nature* **530**, 481–484 (2016).
9. M. Mahgoub *et al.*, MeCP2 and histone deacetylases 1 and 2 in dorsal striatum collectively suppress repetitive behaviors. *Nat. Neurosci.* **19**, 1506–1512 (2016).
10. L. R. Mangieri *et al.*, A neural basis for antagonistic control of feeding and compulsive behaviors. *Nat. Commun.* **9**, 52 (2018).
11. M. D. Mu *et al.*, A limbic circuitry involved in emotional stress-induced grooming. *Nat. Commun.* **11**, 2261 (2020).
12. B. Terzic *et al.*, Temporal manipulation of *Cdkl5* reveals essential postdevelopmental functions and reversible *CDKL5* deficiency disorder-related deficits. *J. Clin. Invest.* **131**, e143655 (2021).
13. M. Ullrich *et al.*, OCD-like behavior is caused by dysfunction of thalamo-amygdala circuits and upregulated *TrkB/ERK-MAPK* signaling as a result of *SPRED2* deficiency. *Mol. Psychiatry* **23**, 444–458 (2018).
14. W. Hong, D. W. Kim, D. J. Anderson, Antagonistic control of social versus repetitive self-grooming behaviors by separable amygdala neuronal subsets. *Cell* **158**, 1348–1361 (2014).
15. O. M. Folkes *et al.*, An endocannabinoid-regulated basolateral amygdala-nucleus accumbens circuit modulates sociability. *J. Clin. Invest.* **130**, 1728–1742 (2020).
16. Z. Xie *et al.*, A brain-to-spinal sensorimotor loop for repetitive self-grooming. *Neuron* **110**, 874–890.e7 (2022).
17. S. P. Whiteside, J. D. Port, J. S. Abramowitz, A meta-analysis of functional neuroimaging in obsessive-compulsive disorder. *Psychiatry Res.* **132**, 69–79 (2004).
18. T. Nakao, K. Okada, S. Kanba, Neurobiological model of obsessive-compulsive disorder: Evidence from recent neuropsychological and neuroimaging findings. *Psychiatry Clin. Neurosci.* **68**, 587–605 (2014).
19. Y. F. Zhang *et al.*, Ventral striatal islands of Calleja neurons control grooming in mice. *Nat. Neurosci.* **24**, 1699–1710 (2021).
20. S. Saxena, R. G. Bota, A. L. Brody, Brain-behavior relationships in obsessive-compulsive disorder. *Semin. Clin. Neuropsychiatry* **6**, 82–101 (2001).
21. S. R. Chamberlain *et al.*, Orbitofrontal dysfunction in patients with obsessive-compulsive disorder and their unaffected relatives. *Science* **321**, 421–422 (2008).
22. J. Y. Rotge *et al.*, Meta-analysis of brain volume changes in obsessive-compulsive disorder. *Biol. Psychiatry* **65**, 75–83 (2009).
23. M. R. Milad, S. L. Rauch, Obsessive-compulsive disorder: Beyond segregated cortico-striatal pathways. *Trends Cogn. Sci.* **16**, 43–51 (2012).
24. G. Krabbe *et al.*, Microglial *NF κ B-TNF α* hyperactivation induces obsessive-compulsive behavior in mouse models of progranulin-deficient frontotemporal dementia. *Proc. Natl. Acad. Sci. U.S.A.* **114**, 5029–5034 (2017).
25. S. E. Ahmari *et al.*, Repeated cortico-striatal stimulation generates persistent OCD-like behavior. *Science* **340**, 1234–1239 (2013).
26. E. Burguière, P. Monteiro, G. Feng, A. M. Graybiel, Optogenetic stimulation of lateral orbitofronto-striatal pathway suppresses compulsive behaviors. *Science* **340**, 1243–1246 (2013).
27. K. C. Berridge, J. W. Aldridge, Super-stereotypy II: Enhancement of a complex movement sequence by intraventricular dopamine D1 agonists. *Synapse* **37**, 205–215 (2000).
28. I. D. Zike *et al.*, OCD candidate gene *SLC1A1/EAAT3* impacts basal ganglia-mediated activity and stereotypic behavior. *Proc. Natl. Acad. Sci. U.S.A.* **114**, 5719–5724 (2017).
29. H. C. Cromwell, K. C. Berridge, J. Drago, M. S. Levine, Action sequencing is impaired in *D1A*-deficient mutant mice. *Eur. J. Neurosci.* **10**, 2426–2432 (1998).
30. C. J. McDougle, C. N. Epperson, G. H. Pelton, L. H. Price, A double-blind, placebo-controlled study of risperidone addition in serotonin reuptake inhibitor-refractory obsessive-compulsive disorder. *Arch. Gen. Psychiatry* **57**, 794–801 (2000).
31. W. R. Stauffer *et al.*, Dopamine neuron-specific optogenetic stimulation in rhesus macaques. *Cell* **166**, 1564–1571.e6 (2016).
32. M. J. M. Murphy, A. Y. Deutch, Organization of afferents to the orbitofrontal cortex in the rat. *J. Comp. Neurol.* **526**, 1498–1526 (2018).
33. E. Burguière, P. Monteiro, L. Mallet, G. Feng, A. M. Graybiel, Striatal circuits, habits, and implications for obsessive-compulsive disorder. *Curr. Opin. Neurobiol.* **30**, 59–65 (2015).
34. C. J. McDougle *et al.*, Risperidone for the core symptom domains of autism: Results from the study by the autism network of the research units on pediatric psychopharmacology. *Am. J. Psychiatry* **162**, 1142–1148 (2005).
35. D. Ducas *et al.*, D2 and D3 dopamine receptor affinity predicts effectiveness of antipsychotic drugs in obsessive-compulsive disorders: A meta-regression analysis. *Psychopharmacology (Berl.)* **231**, 3765–3770 (2014).
36. D. J. Stein *et al.*, Obsessive-compulsive disorder. *Nat. Rev. Dis. Primers* **5**, 52 (2019).
37. M. Xu *et al.*, Basal forebrain circuit for sleep-wake control. *Nat. Neurosci.* **18**, 1641–1647 (2015).
38. K. Lee *et al.*, Parvalbumin interneurons modulate striatal output and enhance performance during associative learning. *Neuron* **99**, 239 (2018).
39. P. Anikeeva *et al.*, Optetrode: A multichannel readout for optogenetic control in freely moving mice. *Nat. Neurosci.* **15**, 163–170 (2011).
40. D. F. English *et al.*, GABAergic circuits mediate the reinforcement-related signals of striatal cholinergic interneurons. *Nat. Neurosci.* **15**, 123–130 (2011).
41. Y. Senai, G. Buzsáki, Physiological properties and behavioral correlates of hippocampal granule cells and mossy cells. *Neuron* **93**, 691–704.e5 (2017).
42. S. Fujisawa, A. Amarasingham, M. T. Harrison, G. Buzsáki, Behavior-dependent short-term assembly dynamics in the medial prefrontal cortex. *Nat. Neurosci.* **11**, 823–833 (2008).
43. S. El-Boustani *et al.*, Anatomically and functionally distinct thalamocortical inputs to primary and secondary mouse whisker somatosensory cortices. *Nat. Commun.* **11**, 3342 (2020).
44. B. Zingg *et al.*, AAV-mediated anterograde transsynaptic tagging: Mapping corticocollicular input-defined neural pathways for defense behaviors. *Neuron* **93**, 33–47 (2017).
45. D. G. Tervo *et al.*, A designer AAV variant permits efficient retrograde access to projection neurons. *Neuron* **92**, 372–382 (2016).
46. D. H. Kang *et al.*, Volumetric investigation of the frontal-subcortical circuitry in patients with obsessive-compulsive disorder. *J. Neuropsychiatry Clin. Neurosci.* **16**, 342–349 (2004).
47. P. R. Szeszko *et al.*, Brain structural abnormalities in psychotropic drug-naïve pediatric patients with obsessive-compulsive disorder. *Am. J. Psychiatry* **161**, 1049–1056 (2004).

48. D. Robinson *et al.*, Reduced caudate nucleus volume in obsessive-compulsive disorder. *Arch. Gen. Psychiatry* **52**, 393–398 (1995).
49. J. W. Aldridge, K. C. Berridge, A. R. Rosen, Basal ganglia neural mechanisms of natural movement sequences. *Can. J. Physiol. Pharmacol.* **82**, 732–739 (2004).
50. J. Sjöbom, M. Tamtö, P. Halje, I. Brys, P. Petersson, Cortical and striatal circuits together encode transitions in natural behavior. *Sci. Adv.* **6**, eabc1173 (2020).
51. B. D. Greenberg, S. L. Rauch, S. N. Haber, Invasive circuitry-based neurotherapeutics: Stereotactic ablation and deep brain stimulation for OCD. *Neuropsychopharmacology* **35**, 317–336 (2010).
52. T. Sesia, B. Bizup, A. A. Grace, Nucleus accumbens high-frequency stimulation selectively impacts nigrostriatal dopaminergic neurons. *Int. J. Neuropsychopharmacol.* **17**, 421–427 (2014).
53. M. A. Jenike, Clinical practice. Obsessive-compulsive disorder. *N. Engl. J. Med.* **350**, 259–265 (2004).
54. G. Maina, E. Pessina, U. Albert, F. Bogetto, 8-week, single-blind, randomized trial comparing risperidone versus olanzapine augmentation of serotonin reuptake inhibitors in treatment-resistant obsessive-compulsive disorder. *Eur. Neuropsychopharmacol.* **18**, 364–372 (2008).
55. G. Goodwin *et al.*, Advantages and disadvantages of combination treatment with antipsychotics ECNP Consensus Meeting, March 2008, Nice. *Eur. Neuropsychopharmacol.* **19**, 520–532 (2009).
56. A. V. Kalueff *et al.*, Neurobiology of rodent self-grooming and its value for translational neuroscience. *Nat. Rev. Neurosci.* **17**, 45–59 (2016).
57. J. Alsö *et al.*, Dopamine D2-like receptor stimulation blocks negative feedback in visual and spatial reversal learning in the rat: Behavioural and computational evidence. *Psychopharmacology (Berl.)* **236**, 2307–2323 (2019).
58. N. K. Horst, B. Jupp, A. C. Roberts, T. W. Robbins, D2 receptors and cognitive flexibility in marmosets: Tri-phasic dose-response effects of intra-striatal quinpirole on serial reversal performance. *Neuropsychopharmacology* **44**, 564–571 (2019).
59. D. M. Eagle *et al.*, Dissociable dopaminergic and pavlovian influences in goal-trackers and sign-trackers on a model of compulsive checking in OCD. *Psychopharmacology (Berl.)* **237**, 3569–3581 (2020).
60. J. L. Seiler *et al.*, Dopamine signaling in the dorsomedial striatum promotes compulsive behavior. *Curr. Biol.* **32**, 1175–1188.e5 (2022).
61. S. Lammel *et al.*, Unique properties of mesoprefrontal neurons within a dual mesocorticolimbic dopamine system. *Neuron* **57**, 760–773 (2008).
62. K. T. Beier *et al.*, Circuit architecture of VTA dopamine neurons revealed by systematic input-output mapping. *Cell* **162**, 622–634 (2015).
63. S. B. Wolff *et al.*, Amygdala interneuron subtypes control fear learning through disinhibition. *Nature* **509**, 453–458 (2014).